THE JOURNAL OF PHYSICAL CHEMISTRY C

Article

pubs.acs.org/JPCC

Growth of Two-Dimensional Lithium Islands on CaO(001) Thin Films

Xiang Shao,[†] Yi Cui,[†] Wolf-Dieter Schneider,[†,‡] Niklas Nilius,*[,†] and Hans-Joachim Freund[†]

[†]Fritz-Haber-Institut der Max-Planck-Gesellschaft, Faradayweg 4-6, 14195 Berlin, Germany

[‡]Ecole Polytechnique Federale de Lausanne, Institute of Condensed Matter Physics, CH-1015 Lausanne, Switzerland

ABSTRACT: The nucleation and growth behavior of lithium on a CaO/Mo(001) thin film has been investigated by means of scanning tunneling microscopy and spectroscopy. The Li follows two different growth regimes on the surface. Whereas extended 2D islands develop on top of the defect-free CaO terraces, small 3D deposits decorate a network of domain boundaries that is present in the oxide film. The 2D islands have metallic character, as deduced from a standing wave pattern observed on their surface at low-bias. In contrast, a cationic nature is proposed for the defect-bound 3D species as a result of an electron-transfer from the Li 2s valence orbital into trap states localized in the CaO line defects. Tunneling spectroscopy reveals an unoccupied gap state below the CaO conduction band that originates from Li−O hybridization across the metal-oxide interface. With increasing diameter of the Li islands, this state shifts toward the Fermi level, reflecting the decreasing workfunction at higher Li coverage.

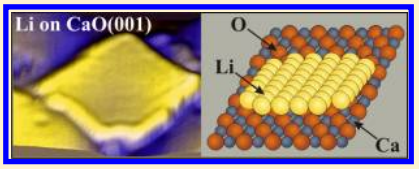

INTRODUCTION

The adsorption of alkali metals on oxide surfaces has model-character for elucidating the interactions at metal-oxide interfaces and is therefore in the focus of experimental[1−4] and theoretical[5−7] studies for several decades already. The alkalis are most suited to gain insight into fundamental processes at metal-oxide interfaces due to their ideal free-electron character and low ionization potential. The latter renders electron donation from the singly occupied alkali $n\bullet s^1$ orbital likely and enables a detailed exploration of charge-transfer processes that accompany binding to the oxide surface.[6−8] Owing to the specific nature of alkali−oxide interactions, alkali deposition onto wide-gap insulators often leads to the formation of extended monolayer metal sheets that are effectively decoupled from the substrate beneath.[4,9] Various fascinating effects have been assigned to such systems, such as giant electron−phonon coupling triggering structural distortions in the 2D layers,[10] band gap openings at the Fermi level (E_F), and electron quantization effects in the confined metal sheets.[11] From an applied point of view, the alkali systems play an important role for promoting reactions in heterogeneous catalysis[12,13] and for the development of the next generation of solar cells and gas sensors.[14,15]

The interactions between alkali metals and oxide surfaces can be divided into two regimes, depending on the reducibility and ionicity of the oxide support. Whereas adsorption on reducible, small-gap oxides is dominated by the formation of covalent bonds associated with a substantial charge transfer to nearby cations,[6,7] electrostatic, and polarization forces govern the interaction with strongly ionic, wide-gap materials.[5,16] On the TiO_2(110) surface, for example, alkali atoms bind to oxygen hollow sites by donating their valence s electron to adjacent Ti^{4+} species.[6,7] On MgO(001), no charge transfer takes place, and the alkali atoms preferentially attach to O top positions via electrostatic coupling.[8] As a result, the typical binding energies of alkali atoms are twice as large on reducible compared to nonreducible oxides, for example, 2.4 eV for Na/TiO_2[7] but only 1.0 eV for Na/MgO.[17]

Most of the experimental data on the interplay of alkali metals with oxide surfaces have been derived from nonlocal electron-spectroscopy and workfunction measurements.[2,3,19] In addition, electron paramagnetic resonance spectroscopy was employed to deduce charge-transfer processes out of the alkali species,[18] whereas single-crystal calorimetry techniques were applied to analyze the binding strength of alkalis to MgO (001).[4] Scanning tunneling microscopy (STM), on the other hand, is rarely used, most likely because of the limited conductance of many oxides and difficulties to image the alkali species on their surface.[1,9,19,20] Moreover, special care is required to guarantee the cleanliness of such systems and to avoid misinterpretations of the STM images due to residual gases adsorbed on the reactive alkali metals.

In this article, we present an STM study on the adsorption behavior of lithium on Mo(001)-supported CaO thin films. We find the Li growth to be predominately 2D-like on this surface, giving rise to the formation of large metal sheets with monolayer height. STM conductance spectroscopy indicates the metallicity of the alkali ad-layer and reveals a gradual workfunction decrease with increasing Li coverage.

EXPERIMENTAL SECTION

The experiments have been carried out with a custom-built STM setup operated at 10 K, which is embedded in an ultrahigh vacuum chamber (2×10^{-10} mbar) equipped with standard tools for sample preparation and analysis. Whereas the surface morphology was deduced from constant-current images, insight into the electronic structure was obtained with differential conductance spectroscopy performed with lock-in

Received: June 27, 2012
Revised: August 1, 2012
Published: August 1, 2012

   dx.doi.org/10.1021/jp306328c | J. Phys. Chem. C 2012, 116, 17980−17984

technique (10 mV rms/1147 Hz modulation bias). CaO films of ~15 ML thickness were prepared by reactive Ca deposition in 5×10^{-7} mbar O_2 onto a sputtered/annealed Mo(001) single crystal.[21] After deposition, the films were annealed to 1000 K to stimulate crystallization. The CaO stabilizes in the rocksalt structure with the (001) surface exposed, as deduced from the square (1×1) LEED pattern. Directly at the interface, a mixed Ca−Mo oxide develops with 25% of the Ca ions being replaced by interdiffusing Mo.[22] Because the Mo−O bond length is shorter than the Ca−O distance, the mixed phase has a reduced lattice parameter than pure CaO(001) and exhibits a better lattice match with the Mo(001) surface. Pristine CaO only develops beyond 5 ML nominal thickness, when the Mo diffusion becomes insufficient to stabilize the mixed phase.[21] Whereas isolated CaO patches nucleate first on top of the wetting layer, a closed film develops above 15 ML thickness. The final film contains a network of domain boundaries, being the remnants of the original island-edges. Annihilation of these line defects is inhibited by the out-of-phase crystallographic relation between neighboring oxide grains. The domain boundaries preferentially orient along the nonpolar CaO⟨100⟩ direction and enclose single-crystalline oxide terraces of 10−20 nm size (Figure 1a). In a last step, Li was

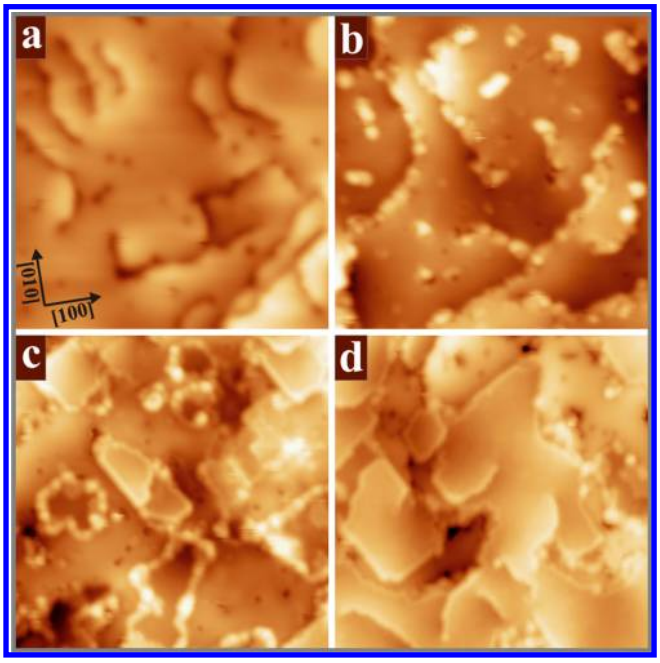

Figure 1. STM topographic images of 15 ML CaO/Mo(001) films after increasing the Li coverage from (a) 0 ML, (b) 0.05 ML, (c) 0.3 ML, to (d) 0.6 ML (50×50 nm^2, 2.8 V).

dosed from a commercial SAES getter onto the freshly prepared films at 300 K. The surface coverage was varied between 0.05 and 1 ML with one monolayer referring to one Li atom per surface O ion in CaO(001), that is, to 8.65×10^{14} atoms/cm^{-2}.

RESULTS AND DISCUSSION

Structure and Morphology of Li Deposits. Deposition of 0.05 ML Li results in the formation of small, irregularly shaped deposits located on the terraces and line defects of the oxide film (Figure 1b). Their apparent height has been determined to be 0.25 nm at 4.0 V sample bias, whereas their surface density amounts to 1×10^{12} cm^{-2}. With increasing Li exposure, mainly the terrace-bound deposits transform into extended, planar islands, whereas clusters along the defect lines remain small and structurally ill-defined. At 0.3 ML nominal coverage, the planar ad-islands reach around 10 nm diameter and develop straight edges parallel to the CaO⟨110⟩ direction. Conversely, the defect-bound clusters grow mainly in number and not in size, producing characteristic 'encircled' regions, as seen in Figure 1c (left). An almost complete alkali ad-layer is obtained after dosing 1 ML of Li. At this coverage, only small CaO patches remain detectable, as identified by their uneven and defective appearance, whereas most of the surface is covered with a homogeneous metal overlayer (Figure 1d).

Electron transport through the thick CaO films requires a minimum bias of +4.0 V, reflecting the 8.0 eV band gap of the oxide material.[21] However, this constraint disappears on top of large Li islands that develop enough metallicity to enable low-bias imaging, at least for currents below 10 pA. Such measurements provide insight into the atomic structure and the electronic properties of the ad-islands. Figure 2 displays an

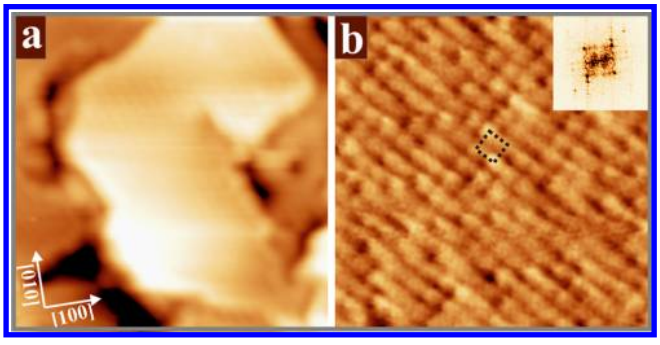

Figure 2. (a) Overview (25×25 nm^2, 2.0 V) and (b) atomically resolved STM image of a large Li island on CaO/Mo(001) (5×5 nm^2, 0.5 V). The dashed square marks the Li unit cell; the inset shows a fast-Fourier-transform of the image.

extended Li island and an associated close-up image showing atomic resolution. The latter reveals a square lattice that runs along the CaO⟨110⟩ directions and has 0.34 nm interatomic spacing. A fast-Fourier-transform (FFT) of this image reproduces both the square symmetry and size of the Li unit cell. On the basis of this data, a structure model for the Li ad-layer on CaO(001) is proposed. The experimental Li unit-cell matches the dimension of the CaO primitive cell, suggesting an epitaxial relationship achieved by compressing the bulk Li lattice parameter (0.351 nm) by 3%. We expect the Li atoms to occupy anionic sites in the CaO surface and to form acid−base pairs.[17] According to previous DFT calculations, the interaction is driven by mutual polarization of the Li and oxygen atoms with small contributions from interfacial hybridization and charge transfer.[5] The associated binding energy has been given with 1.6 eV per Li atom in a monolayer but drops below 1.0 eV for less compact Li arrangements, such as a 2×2 configuration.[5] Similar results are reported for other alkali metals on CaO(001) and the iso-structural MgO(001) support.[8,16] Also there, the binding to surface O ions is highly preferred, and the respective energies increase from below 1 eV for isolated atoms to 1.5 eV for compact layers. This evolution reflects the stabilizing effect of metal−metal bonds upon island formation. Interestingly, most of the studies suggest a 2D growth of alkali metals on CaO and MgO surfaces, despite the

dx.doi.org/10.1021/jp306328c | J. Phys. Chem. C 2012, 116, 17980−17984

weak interface coupling.[4,16] One reason is the small cohesion inside the alkali metals, as evident from their low melting temperature, which produces only a weak thermodynamic incentive for 3D growth. Also, kinetic obstacles might be relevant and DFT calculations found indeed a substantial barrier for Li up-diffusion from the MgO surface to a preexisting Li island, which might not be overcome at room temperature.[16] This assumption is supported by an experimental observation that 2D Li islands on MgO(001) turn 3D upon annealing to 500 K.[9]

We exclude that charge-transfer processes across the metal-oxide interface are responsible for the 2D Li growth, although similar concepts have been utilized to explain the formation of planar gold islands on MgO and CaO films.[23,24] As shown in recent EPR[18] and DFT studies,[5,8] Li remains neutral on bulk oxides, as no electron traps are available in the ideal rocksalt lattices. Charge transfer out of the Li species might still be possible in the limit of ultrathin films, as the metal support beneath provides empty states to accept the Li electrons. However, the 15 ML-thick CaO films used here are likely too thick to allow for direct electron tunneling from the Li into the Mo support. Moreover, the low workfunction of the CaO/Mo(001) system renders electron transfer into the substrate energetically unfavorable.[25] We will provide further evidence for the metallic nature of the Li islands later in the article.

Finally, we comment on the efficient growth of Li islands on the CaO terraces, which contrasts with clusters on the line defects that hardly increase in size upon continued Li exposure (Figure 1b,c). We ascribe this effect to a charging of the defect-bound aggregates via electron transfer into trap states located in the CaO defect lines beneath.[26,27] This leads to a gradual increase of the internal Coulomb repulsion in the deposits that causes the particle growth to cease at a certain point. Because similar charging effects are absent on the plain oxide terraces, the ad-islands continue to grow in these positions. This has the interesting consequence that Li growth proceeds from the defect-poor terraces and not from the grain boundaries, in contrast with the behavior found for most noble and transition metals.[28]

Electronic Properties of Li Deposits. Insight into the sample electronic structure was obtained from bias-dependent topographic images and dI/dV spectroscopy. Figure 3a shows a bias series of a medium-sized Li island (area: 60 nm^2). At +1.0 V, the island elevates by 0.1 nm above the CaO surface and is surrounded by a bright, 0.25 nm high rim. Its surface is covered with a small number of uniform protrusions, being tentatively assigned to Li atoms that were unable to leave the top-facet due to a Schwoebel barrier for step-down diffusion.[16,29] Alternatively, the ad-species might be molecules from the rest gas, for example, H_2O, that got stuck onto the reactive Li surface. At +1.8 V, the island suddenly turns bright and its apparent height increases to 0.25 nm with respect to the CaO film. Evidently, an electronic state becomes accessible at this bias that represents a new transport channel for the tunneling electrons.[11] The associated tip-retraction from the surface diminishes the visibility of tiny topographic details on the Li island and renders its top-facet more homogeneous. Interestingly, the critical bias for a transition between dim and bright appearance sensitively depends on the Li dose. Whereas for 0.2 ML nominal coverage it occurs at ~1.5 V, it downshifts to 0.5 V at 0.6 ML coverage, as exemplified in Figure 3b.

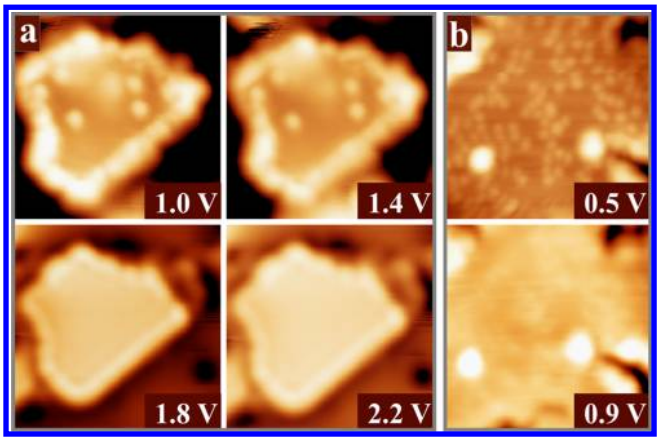

Figure 3. Topographic images (15 × 15 nm^2) of (a) a medium and (b) a large Li island taken at the indicated sample bias. Note the switch between dim and bright appearance of the islands above 1.5 and 0.5 V in panels a and b, respectively.

At even lower bias, a ripple-pattern becomes detectable on top of the Li islands, which is readily assigned to charge-density waves arising from scattering of a free-electron-like state at structural perturbations (Figure 4).[30] A FFT analysis of such images produces a ring-like feature of 2.52 nm^{-1} diameter that reflects the Fermi contour of the respective electronic state.[31] Given its circular appearance in reciprocal space, it is identified as an isotropic, s-like electron band (the Li 2s). The size of the contour is independent of the bias voltage in topographic images because of the dominance of Fermi electrons for scattering.[32] Unfortunately, state-selective dI/dV maps could not be acquired in our experiment due to strong limitations in the tunnel current, and no dispersion relation could be determined for the electronic state. The low-bias scattering pattern still contains useful information on the metallicity of the Li islands. From the diameter of the FFT contour, the Fermi wave-vector is determined to be 10.1 nm^{-1}, which compares to 11.6 nm^{-1}, as calculated from the Fermi energy of bulk lithium with a free-electron model.[33] The good match of both values indicates that a metallic Li system has established already in the monolayer islands. Moreover, a substantial charge transfer out of the ad-structures or even a full Li ionization can be excluded because this would cause the Fermi surface to shrink or disappear. We note that the development of metallic properties in spatially confined Li islands is in full agreement with the ideal free-electron nature of the Li 2s conduction states.

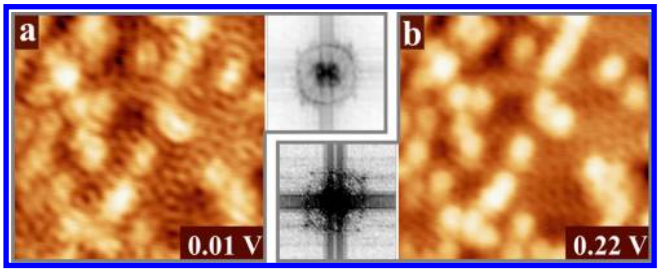

Figure 4. Topographic images (10 × 10 nm^2) taken on top of a large Li island at (a) 10 and (b) 220 mV. The interference patterns in the images transform into the same circular contour in the respective FFT plots (insets).

Further insight into the Li electronic structure is obtained from dI/dV spectra taken on two differently sized islands (Figure 5). The spectrum of the smaller one (area: 15 nm^2)

dx.doi.org/10.1021/jp306328c | J. Phys. Chem. C 2012, 116, 17980−17984

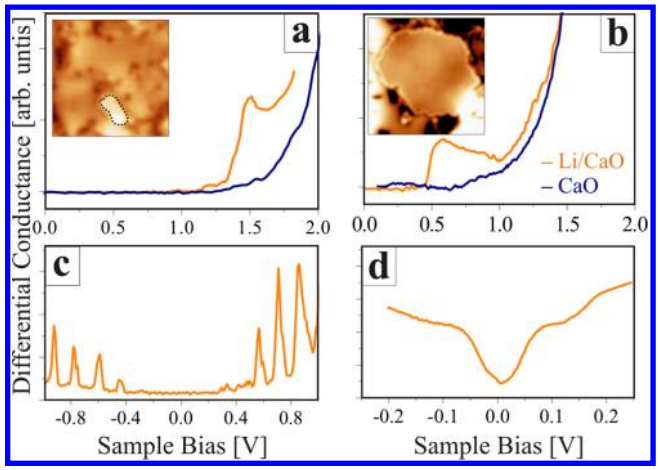

Figure 5. (a,b) Differential conductance spectra taken in the center of the two Li islands shown in the insets (30 × 30 nm^2). The bias set-point was adjusted to 1.8 V. (c,d) Spectra on the same islands but taken in a smaller bias window (set-points of 1.0 and 0.25 V). Whereas the spectral features in panels a and b are intrinsic to the Li/CaO system, the ones in panels c and d are due to Coulomb charging effects.

shows a prominent shoulder at 1.5 V, which is 0.5 V below the CaO conduction-band onset. The larger island (180 nm^2) shows a comparable spectral feature at 0.6 V, although also the oxide band has downshifted to 1.5 V in this case. Other Li islands exhibit similar spectral features, that is, a split-off state below the CaO conduction band that moves toward E_F with increasing island size. Remarkably, the dI/dV shoulder always occurs at the same bias at which the islands turn bright in the topographic images, indicating a direct correlation between the respective electronic state and the contrast change (Figure 3). We doubt that the detected energy level is intrinsic to lithium, as the next states above the Li 2s (the Li 2p) should be much higher in energy. We rather suggest that the spectral feature originates from a coupling of metal and oxide electronic states across the interface. For the proposed Li-on-O registry, the coupling will involve mainly the Li 2s and O 2p states, producing filled O- and empty Li-dominated resonances inside the gap.[34] In our case, only the latter is detected as split-off state of the CaO conduction band. Note that similar interface states were identified for a reverse structure, in which a single MgO layer was put on top of a Ag(001) surface.[35]

The downshift of the interface state and the CaO main bands with higher Li load indicates a gradual reduction of the vacuum energy in front of the Li-coated surface (Figure 5).[36] The effect is driven by the low Li workfunction that is just 2.9 eV in the bulk limit[37] and hence 1.1 eV lower than the CaO/Mo value. The shift mainly affects the interface state with its high surface localization, whereas the CaO bands experience a smaller change due to their position below the Li ad-layer. The workfunction decrease would be even larger if a substantial fraction of the Li would ionize upon adsorption.[38,39] However, as demonstrated above, the monolayer islands are largely metallic, and only the defect-bound clusters may contain cationic Li species. A distinction between Li^0 and Li^+ would be feasible with a systematic workfunction study performed as a function of the Li load, which is, however, beyond the scope of this work.

Finally, equidistant dI/dV peaks were revealed in the Li but not in the oxide spectra when stabilizing the tip at lower bias, hence inside the CaO band gap (Figure 5c,d). The spacing of the maxima was found to decrease from 150 to 50 mV when increasing the island size from 15 to 100 nm^2, respectively. For even larger patches, the regular peak sequence disappeared and only a broad dI/dV minimum was detected at zero bias. These spectral phenomena are readily identified as Coulomb staircase (the equidistant peaks) and Coulomb blockade (the zero-bias dip), introduced by the double-barrier nature of our tunnel junction that consist of a vacuum and an oxide gap.[40−42] Tunneling electrons have to enter the Li islands on their way between tip and sample, a process that is inhibited by the Coulomb repulsion exerted by electrons in the confined electronic system. Distinct dI/dV peaks are now detected whenever the incoming electrons have sufficient energy to overcome this barrier and the number of extra charges per island increases by one. The charging energy depends inversely on the capacitance of the two transport channels, which in turn scales with the island size.[40] Consequently, the spacing between neighboring peaks becomes smaller in larger islands and only a single dI/dV dip develops in the limit of very large patches (Figure 5c,d).

■ CONCLUSIONS

The growth and electronic properties of lithium on CaO(001) films have been analyzed by STM. Lithium grows epitaxially by forming Li−O interface bonds and spreads into large 2D islands. Only at defect sites, such as grain boundaries, are small 3D particles detected. The ad-islands are metallic, as revealed from their free-electron-like scattering response observed in low-bias STM images. At higher positive bias, an empty Li−CaO interface state is detected that gradually moves toward E_F with increasing island size. This downshift is ascribed to a workfunction decrease induced by the Li ad-metal and affects the CaO band edges as well. Given their monolayer nature, the Li islands represent an interesting model system to study 2D metals that are expected to display unique electronic and phononic properties. In addition, Li-induced band-bending effects might be exploited to tailor the properties of the CaO film beneath, for example, by producing charge accumulation zones close to the interface. The experiments discussed here form a solid ground for future studies along this line.

■ AUTHOR INFORMATION

Corresponding Author

*E-mail: nilius@fhi-berlin.mpg.de.

Notes

The authors declare no competing financial interest.

■ ACKNOWLEDGMENTS

Financial support from the DFG Excellence-Initiative 'Unicat' is gratefully acknowledged.

■ REFERENCES

(1) (a) Onishi, H.; Aruga, T.; Egawa, C.; Iwasawa, Y. *Surf. Sci.* **1988**, *199*, 54−66. (b) Onishi, H.; Iwasawa, Y. *Catal. Lett.* **1996**, *38*, 89−94.
(2) Lagarde, P.; Flank, A.-M.; Prado, R. J.; Bourgeois, S.; Jupille, J. *Surf. Sci.* **2004**, *553*, 115−125.
(3) Krischok, S.; Schaefer, J. A.; Hofft, O.; Kempter, V. *Surf. Interface Anal.* **2005**, *37*, 83−89.
(4) Farmer, J. A.; Campbell, C. T.; Xu, L.; Henkelman, G. *J. Am. Chem. Soc.* **2009**, *131*, 3098−3103.
(5) Alfonso, D. R.; Jaffe, J. E.; Hess, A. C.; Gutowski, M. *Surf. Sci.* **2000**, *466*, 111−118.

(6) San Miguel, M. A.; Calzado, C. J.; Sanz, J. F. *J. Phys. Chem. B* **2001**, *105*, 1794−1798.
(7) Albaret, T.; Finocchi, F.; Noguera, C.; De Vita, A. *Phys. Rev. B* **2001**, *65*, 035402.
(8) Finazzi, E.; Di Valentin, C.; Pacchioni, G.; Chiesa, M.; Giamello, E.; Gao, H.; Lian, J.; Risse, T.; Freund, H.-J. *J. Chem. Eur. J.* **2008**, *14*, 4404−4414.
(9) Myrach, P.; Nilius, N.; Levchenko, S. V.; Gonchar, A.; Risse, T.; Dinse, K.-P.; Boatner, L. A.; Frandsen, W.; Horn, R.; Freund, H.-J.; Schlögl, R.; Scheffler, M. *ChemCatChem* **2010**, *2*, 854−862.
(10) Fasolino, A.; Los, J. H.; Katsnelson, M. I. *Nat. Mater.* **2007**, *6*, 858−861.
(11) Lin, X.; Nilius, N.; Freund, H.-J.; Walter, M.; Frondelius, P.; Honkola, H.; Häkkinen, H. *Phys. Rev. Lett.* **2009**, *102*, 206801.
(12) *Handbook of Heterogeneous Catalysis*; Ertl, G., Knoezinger, H., Schueth, F., Weitkamp, J., Eds.; Wiley-VCH: Weinheim, Germany, 2008.
(13) (a) Ito, T.; Wang, J. X.; Lin, C. H.; Lunsford, J. H. *J. Am. Chem. Soc.* **1985**, *107*, 5062−5068. (b) Lunsford, J. H. *Ang. Chem. Int. Ed.* **1995**, *34*, 970−980.
(14) Kumar, D.; Ali, A. *Energy Fuels* **2010**, *24*, 2091−2097.
(15) (a) Liu, Y.; Hagfeldt, A.; Xiao, X.-R.; Lindquist, S.-E. *Sol. Energy Mater. Sol. Cells* **1998**, *55*, 267−281. (b) Traversa, E. *Sens. Actuators, B* **1995**, *23*, 135−156.
(16) (a) Xu, L.-J.; Henkelman, G. *Phys. Rev. B* **2008**, *77*, 205404. (b) Xu, L.-J.; Henkelman, G. *Phys. Rev. B* **2010**, *82*, 115407.
(17) Snyder, J. A.; Jaffe, J. E.; Gutowski, M.; Lin, Z.-J.; Hess, A. C. *J. Chem. Phys.* **2000**, *112*, 3014−3022.
(18) Lian, J.-C.; Finazzi, E.; Di Valentin, C.; Risse, T.; Gao, H.-J.; Pacchioni, G.; Freund, H.-J. *Chem. Phys. Lett.* **2008**, *450*, 308−311.
(19) Souda, R.; Hayami, W.; Aizawa, T.; Ishizawa, Y. *Surf. Sci.* **1993**, *285*, 265−274.
(20) Pang, C. L.; Muryn, C. A; Woodhead, A. P.; Raza, H.; Haycock, S. A.; Dhanak, V. R.; Thornton, G. *Surf. Sci.* **2005**, *583*, L147−L152.
(21) Shao, X.; Myrach, P.; Nilius, N.; Freund, H.-J. *J. Phys. Chem. C* **2011**, *115*, 8784−8789.
(22) Shao, X.; Nilius, N.; Myrach, P.; Freund, H.-J.; Martinez, U.; Prada, S.; Giordano, L.; Pacchioni, G. *Phys. Rev. B* **2011**, *83*, 245407.
(23) Pacchioni, G.; Giordano, L.; Baistrocchi, M. *Phys. Rev. Lett.* **2005**, *94*, 226104.
(24) Nilius, N. *Surf. Sci. Rep.* **2009**, *64*, 595−659.
(25) Giordano, L.; Cinquini, F.; Pacchioni, G. *Phys. Rev. B* **2006**, *73*, 045414.
(26) McKenna, K. P.; Shluger, A. L. *Nat. Mater.* **2008**, *7*, 859−862.
(27) Benia, H. M.; Myrach, P.; Gonchar, A.; Risse, T.; Nilius, N.; Freund, H.-J. *Phys. Rev. B* **2010**, *81*, 241415(R).
(28) Benedetti, S.; Myrach, P.; di Bona, A.; Valeri, S.; Nilius, N.; Freund, H.-J. *Phys. Rev. B* **2011**, *83*, 125423.
(29) (a) Schwoebel, R. L.; Shipsey, E. J. *J. Appl. Phys.* **1966**, *37*, 3682−3686. (b) Ehrlich, G.; Hudda, F. G. *J. Chem. Phys.* **1966**, *44*, 1039−1049.
(30) Hasegawa, Y.; Avouris, Ph. *Phys. Rev. Lett.* **1993**, *71*, 1071−1074.
(31) Petersen, L.; Sprunger, P. T.; Hofmann, P.; Laegsgaard, E.; Briner, B. G.; Doering, M.; Rust, H. P.; Bradshaw, A. M.; Besenbacher, F.; Plummer, E. W. *Phys. Rev. B* **1998**, *57*, R6858−R6861.
(32) Pivetta, M.; Fabien, S.; Patthey, F.; Pelz, J. P.; Schneider, W. D. *Phys. Rev. B* **2003**, *67*, 193402.
(33) Ashcroft, N. W.; Mermin, N. D. *Solid State Physics*; Saunders: Philadelphia, 1976.
(34) Altieri, S.; Tjieng, S. H.; Sawatzky, G. A. *Phys. Rev. B* **2000**, *61*, 16948−16955.
(35) Schintke, S.; Messerli, S.; Pivetta, M.; Patthey, F.; Libjoulle, L.; Stengel, M.; de Vita, A.; Schneider, W. D. *Phys. Rev. Lett.* **2001**, *87*, 276801.
(36) Jerratsch, J.-F.; Nilius, N.; Freund, H.-J.; Martinez, U.; Giordano, L.; Pacchioni, G. *Phys. Rev. B* **2009**, *80*, 245423.
(37) Hölzl, J.; Schulte, F. K.; Wagner, H. *Solid Surface Physics*; Springer Tracts in Modern Physics; Springer: Berlin, 1979; Vol. *85*.
(38) (a) Langmuir, I.; Kingdon, K. H. *Science* **1923**, *57*, 58−60. (b) Langmuir, I. *J. Am. Chem. Soc.* **1932**, *54*, 2798−2832. (c) Gurney, R. W. *Phys. Rev.* **1935**, *47*, 479−482.
(39) (a) Bonzel, H. P. *Surf. Sci. Rep.* **1987**, *8*, 43−125. (b) Diehl, R. D.; McGrath, R. *Surf. Sci. Rep.* **1996**, *23*, 43−171.
(40) Hanna, A. E.; Tinkham, M. *Phys. Rev. B* **1991**, *44*, 5919−5922.
(41) (a) Sattler, K. *Z. Phys. D* **1991**, *19*, 287−292. (b) Amman, M.; Wilkes, R.; Ben-Jacob, E.; Maker, P. D.; Jaklevic, R. C. *Phys. Rev. B* **1991**, *43*, 1146−1149.
(42) Brun, C.; Muller, K. H.; Hong, I. P.; Patthey, F.; Flindt, C.; Schneider, W. D. *Phys. Rev. Lett.* **2012**, *108*, 126802.